Molecular Cell
Article

An Antisense RNA Inhibits Translation by Competing with Standby Ribosomes

Fabien Darfeuille,[1,3,4] Cecilia Unoson,[1,3] Jörg Vogel,[2] and E. Gerhart H. Wagner[1,*]
[1] Department of Cell and Molecular Biology, Biomedical Center, Uppsala University, Box 596, S-75124 Uppsala, Sweden
[2] RNA Biology Group, Max Planck Institute for Infection Biology, Charitéplatz 1, D-10117 Berlin, Germany
[3] These authors contributed equally to this work.
[4] Present address: INSERM U869, 146 rue Léo Saignat, Bordeaux cedex, F-33076, France.
*Correspondence: gerhart.wagner@icm.uu.se
DOI 10.1016/j.molcel.2007.04.003

SUMMARY

Most antisense RNAs in bacteria inhibit translation by competing with ribosomes for translation initiation regions (TIRs) on nascent mRNA. We propose a mechanism by which an antisense RNA inhibits translation without binding directly to a TIR. The *tisAB* locus encodes an SOS-induced toxin, and IstR-1 is the antisense RNA that counteracts toxicity. We show that full-length *tisAB* mRNA (+1) is translationally inactive and endonucleolytic processing produces an active mRNA (+42). IstR-1 binding inhibits translation of this mRNA, and subsequent RNase III cleavage generates a truncated, inactive mRNA (+106). In vitro translation, toeprinting, and structure mapping suggest that active, but not inactive, *tisAB* mRNAs contain an upstream ribosome loading or "standby" site. Standby binding is required for initiation at the highly structured *tisB* TIR. This may involve ribosome sliding to a transiently open *tisB* TIR. IstR-1 competes with ribosomes by base pairing to the standby site located ~100 nucleotides upstream.

INTRODUCTION

Small noncoding RNAs are found in all kingdoms of life and act primarily as regulators of gene expression. In bacteria, this functional class of RNAs is referred to as small RNAs (sRNAs). In *Escherichia coli*, genome-wide searches have identified >70 chromosomally encoded sRNA genes (Argaman et al., 2001; Chen et al., 2002; Rivas et al., 2001; Vogel et al., 2003; Wassarman et al., 2001), and similar findings are reported in other bacteria. If current trends hold, most sRNAs are antisense RNAs and affect target RNAs—positively or negatively—through base pairing. The many antisense RNAs encoded by bacterial plasmids, transposons, and phages regulate processes vital to the lifestyles of these elements (Wagner et al., 2002), whereas most chromosomally encoded sRNAs appear to be stress-response or virulence gene regulators (Gottesman, 2004; Guillier et al., 2006; Romby et al., 2006; Vogel and Papenfort, 2006).

In terms of mechanisms, much has been learned from studies of plasmid-encoded (Wagner et al., 2002), and more recently from chromosomally encoded, antisense-target RNA systems (Storz et al., 2005; Wagner and Darfeuille, 2006). With rare exceptions, the antisense RNAs of accessory elements are *cis* encoded (antisense and target genes overlap in opposite orientation). Those encoded by chromosomes are usually *trans* encoded (different gene locations). *cis*-encoded antisense RNAs are fully complementary to targets, whereas *trans*-encoded antisense RNAs display limited and often noncontiguous target complementarity. Thus, when base-pairing requirements are relaxed, one sRNA may regulate more than a single target, as is the case with DsrA (Repoila et al., 2003). Conversely, one target can be regulated by a few sRNAs, as shown for *ompA* mRNA (Douchin et al., 2006; Rasmussen et al., 2005; Udekwu et al., 2005; Papenfort et al., 2006), and some reports indicate many targets for single sRNAs—in these cases, evidence for direct regulation is still lacking (Guillier and Gottesman, 2006; Massé and Gottesman, 2002; Papenfort et al., 2006). For most, but not all, *trans*-encoded sRNAs, the Sm-like RNA binding protein Hfq is required for full activity in vivo (Valentin-Hansen et al., 2004).

A survey of known interaction sites suggests that most sRNAs target translation initiation regions (TIRs) by directly base pairing to the Shine-Dalgarno (SD) sequence and/or initiation codon. This applies to MicA, MicC, MicF, OxyS, RyhB, SgrS, and Spot 42 (for a review, see Wagner and Darfeuille [2006]). One can therefore conclude that these RNAs inhibit translation by competing with initiating ribosomes. Additionally, binding of an antisense RNA may induce mRNA decay. In *E. coli*, this is often dependent on RNase E. However, in the few cases in which the "hen and egg" question of primary and secondary effects has been addressed, translational inhibition and mRNA decay could be uncoupled. For instance, SgrS RNA inhibits PtsG protein synthesis even in the absence of induced mRNA decay (Morita et al., 2006). In *Staphylococcus aureus*, RNAIII, encoded by the *agr* locus, regulates many

virulence genes (Romby et al., 2006). This antisense RNA activates translation of α-hemolysin and negatively regulates several surface protein mRNAs. Here, binding of RNAIII interferes with translation initiation, but fully efficient inhibition requires cleavages by the double-strand-specific RNase III (Huntzinger et al., 2005).

Posttranscriptional control in general, and antisense RNA-mediated control in particular, occurs mostly on nascent target RNAs. As mRNAs are being transcribed, initiating ribosomes and sRNAs compete kinetically for access to the same TIR/target. However, some mRNAs are translationally inert and require subsequent refolding or processing to become translated. The best-studied case is the *hok/sok* toxin/antitoxin (TA) system that controls postsegregational killing in plasmid R1 (Gerdes et al., 1997; Gerdes and Wagner, 2007). Here, full-length *hok* mRNA requires processing for translational activation. Because de novo synthesis cannot occur in plasmid-free segregants, the unstable Sok antisense RNA decays rapidly. When the stable full-length *hok* mRNA eventually becomes activated and translated, the cells are killed. Thus, regulation depends here on events that are not cotranscriptional, which therefore also could be the case in other control systems.

We previously reported on an in vivo characterization of a TA system (Vogel et al., 2004), *istR/tisAB* (schematically shown in Figure 1A). This locus encodes an antisense RNA, IstR-1, that prevents inadvertent SOS-induced toxicity, which is dependent on *tisB* expression. IstR-1 (constitutive synthesis) and IstR-2 (LexA controlled) are transcribed from two leftward promoters. These RNAs have the same 3′ ends. IstR-2 is not involved in control of *tisAB*, and its putative function will be reported elsewhere (F.D. and E.G.H.W., unpublished data). The rightward transcript, the ~350 nucleotide (nt)-long *tisAB* mRNA (encoding two putative short peptides), is under LexA control and thus induced by DNA damage/SOS conditions. Upon induction, toxicity is observed. Expression of plasmid-borne *istR-1* rescues cells, identifying IstR-1 as an inhibitor of *tisAB* expression. Toxicity is dependent on *tisB*, but not *tisA*, expression. Base pairing between 21 nt in IstR-1 and a region around the *tisA* AUG, ~100 nt upstream of the *tisB* RBS, is supported by mutational analysis. Binding results in RNase III cleavage and generates a translationally inactive mRNA (+106 in Figure 1); a transgenic mRNA transcribed from position +106 in a Δ*istR/tisAB* strain is nontoxic (Vogel et al., 2004). A minor species (+42; Figure 1) originated from endonucleolytic cleavage by an as yet unidentified endoribonuclease. Its relevance remained obscure prior to this work. Taken together, these results indicate that IstR-1 is an antisense RNA that inhibits translation of the toxic TisB peptide.

Based on these in vivo results, regulation relies on an interaction between IstR-1 and the *tisAB* mRNA far upstream of the TIR at which translation of the toxin must initiate. Thus, this system is one of—so far—a few cases in which an antisense RNA does not directly compete

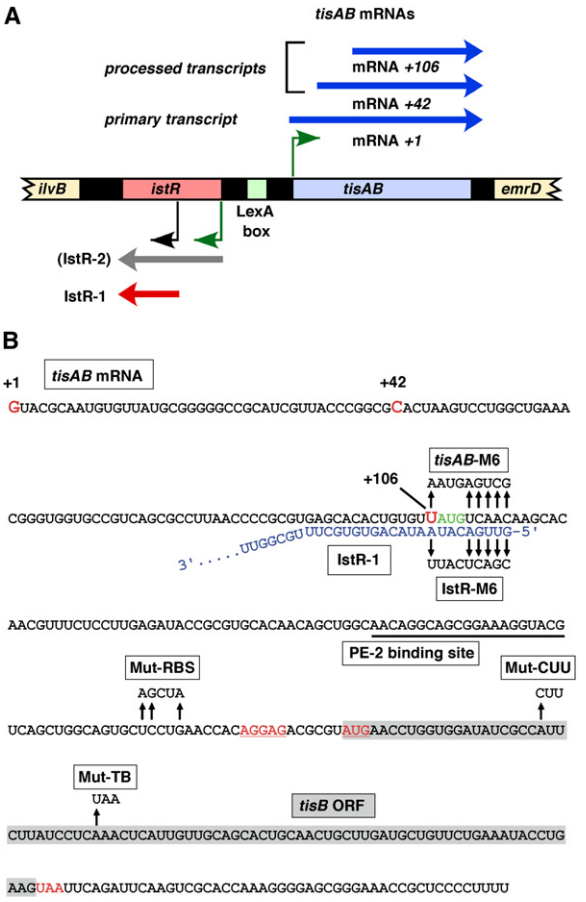

Figure 1. Overview of the *istR/tisAB* Locus

(A) Organization of the locus. Light green box, binding site for the LexA repressor. Green arrowheads, promoters under LexA control; black arrowhead, constitutive promoter. Transcription initiation sites are indicated by arrows. The three different *tisAB* mRNAs previously identified are shown above, and the two IstR RNAs below, the boxed DNA. IstR-2 (gray arrow) is not involved in *tisAB* control.

(B) Sequence of the full-length (+1) *tisAB* mRNA with hallmarks. The first nucleotides of all three (+1, +42, and +106) mRNA species are indicated by red letters. The binding sequence for IstR-1 is shown base paired to the 5′ tail of IstR-1 (blue sequence). Mutations used in this study are depicted with base changes indicated, and the PE2 primer binding site is underlined. The putative start codon of the *tisA* ORF is shown in green (note that *tisA* is not translated, see text). The entire *tisB* reading frame (gray background) is shown with SD, start codon, and stop codon in red letters.

with initiating ribosomes but nevertheless affects translation rather than RNA decay. We propose a new mechanism by which this is accomplished. Two models that might explain distal regulation were ruled out. One of these involved translational coupling between *tisA* and *tisB*, and a second one postulated long-distance changes in secondary structure to affect the accessibility of the *tisB* TIR. Instead, we explain IstR-1-dependent regulation by the ribosome standby model (de Smit and van Duin, 2003). This model accounts for efficient translation initiation at TIRs that are sequestered in stable structures, as

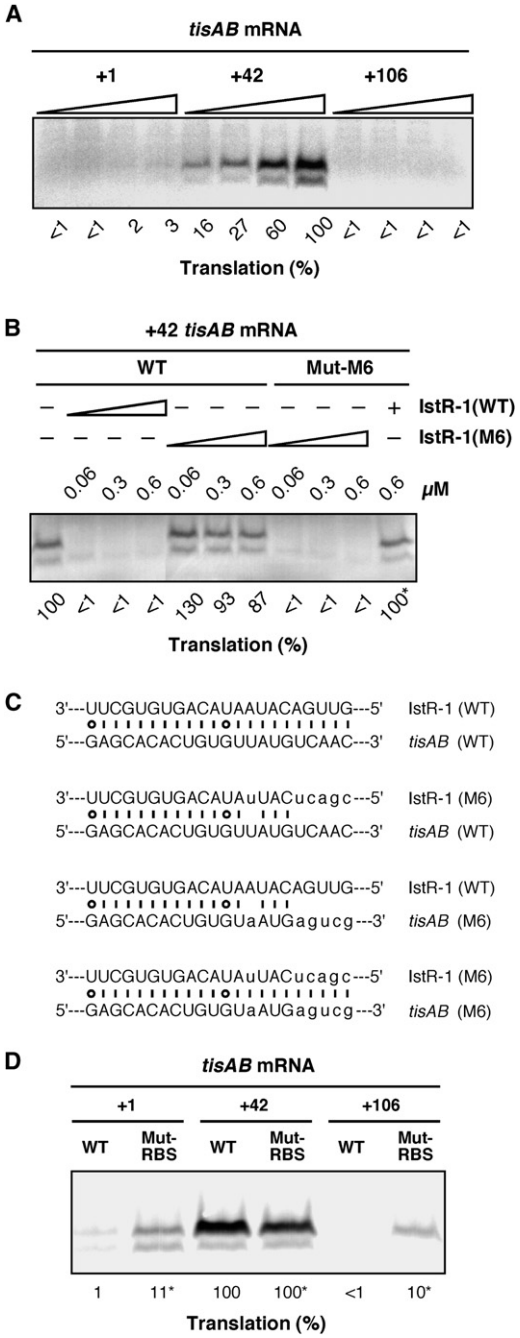

Figure 2. Translation Assays on Wild-Type and Mutant *tisAB* mRNAs

(A) In vitro translation assays with [^{35}S]-Met were carried out as described in the Experimental Procedures at increasing concentrations (left to right: 0.01, 0.02, 0.05, and 0.1 μM) of +1, +42, and +106 *tisAB* mRNAs. Quantification of band intensities gave the translation efficiencies shown below (peak areas of upper bands). The intensity of the band at the highest +42 mRNA concentration was set to 100%.

(B) Translation assays were run with 20 nM *tisAB* +42 mRNA, wild-type, or Mut-M6. When indicated, the antisense RNAs were added at increasing concentrations (μM indicated). [^{35}S]-Met was used for labeling. PhosphorImager-generated images were used for calculation of translation efficiencies (peak areas of upper bands).

(C) Base-pairing schemes for mRNA and IstR-1 sequences (wild-type and Mut-M6). Sequence changes in Mut-M6 are in lowercase.

(D) Comparison of translation yields of +1, +42, and +106 mRNAs generated from wild-type or Mut-RBS DNA templates. The translation yield of the +42 mRNAs was set to 100%, separately, for wild-type and Mut-RBS. For +1 and +106, yields are given in comparison to the corresponding +42 values. Labeling was carried out with [^{14}C]-Leu.

recently demonstrated by elegant biochemical experiments ([Hauryliuk and Ehrenberg, 2006; Studer and Joseph, 2006]; see Discussion). In the context of this work, we suggest that *tisB* translation is inhibited by a strong local secondary structure. In active (+42) *tisAB* mRNA, this inhibition is overcome by the presence of an accessible ribosome loading site (standby site) far upstream. This permits nonspecific ribosome binding, which allows for subsequent sliding into a transiently open *tisB* RBS. Because IstR-1 binds to the standby region, it outcompetes standby ribosomes, thereby preventing *tisB* expression.

RESULTS

Only +42 *tisAB* mRNA Is Translatable In Vitro

The previous in vivo results had identified three *tisAB* mRNA species (Vogel et al., 2004), but their translational activity had not been assessed. To approach a mechanistic understanding, all subsequent experiments were based on RNA species identical to those found in vivo, to test their function under controlled conditions in vitro. First, we asked whether all three mRNA species would support translation. RNAs were synthesized from T7 RNA polymerase promoter-carrying PCR fragments. When the mRNAs were added to the S30 translation extracts, only +42 was efficient as a translation template; two bands are visible in Figure 2A. Surprisingly, the primary *tisAB* transcript, +1, was almost entirely inactive. The +106 mRNA was also translationally inert, in line with its nontoxic in vivo phenotype (Vogel et al., 2004). The differences in translation yield were not due to different rates of RNA degradation in the extract, because all mRNAs were equally stable (data not shown).

Only TisB Is Translated

Because two translation products were observed (strong upper band, weak lower band; Figure 2A), we tested whether they would correspond to TisA and TisB. The two putative peptides should contain 37 (TisA) and 29 amino acids (TisB), respectively. Translation of *tisB* was expected because it is required for toxicity in vivo, whereas translation of *tisA* is not (Vogel et al., 2004). The *tisA* reading frame, unlike that of *tisB*, is not well conserved and lacks a conventional SD sequence (Figure 1B). Because the predicted high α-helical content of TisB made size determinations by migration unreliable, we analyzed the nature of the two translation products by labeling procedures. Figure S1A (in the Supplemental Data available with this article online) shows the presence of

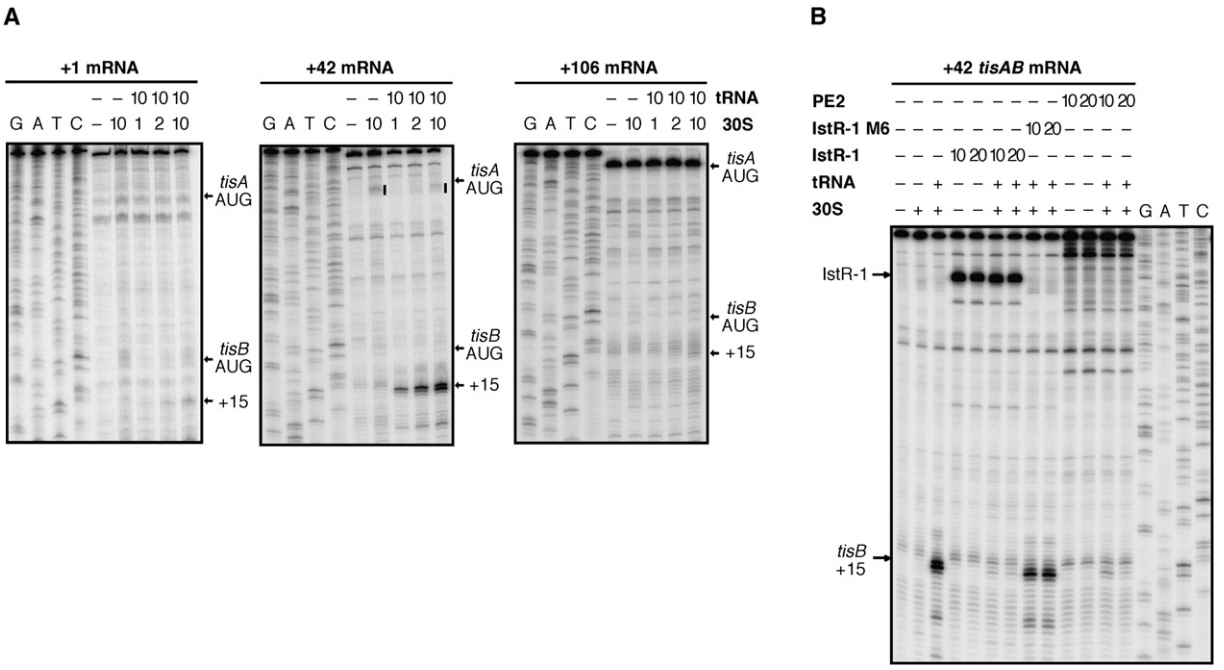

Figure 3. Toeprinting Analysis of *tisAB* mRNAs

(A) Toeprinting was carried out on 2 pmol of +1, +42, and +106 mRNAs as described in the Experimental Procedures. Addition of initiator tRNA (tRNA) and/or 30S subunits is indicated (numbers are pmol added), and GATC refers to sequencing ladders generated with the reverse transcription primer PE1. Reverse transcription stops (toeprints) at position +15 from the *tisB* AUG are highlighted. The approximate position of the *tisA* AUG is shown as well, and a band possibly arising from standby binding is indicated by bars.

(B) The toeprinting protocol was as in (A). Addition of 30S and initiator tRNA, when applicable, was 5 and 10 pmol, respectively. Numbers for competitors (oligo PE2, IstR-1 variants) are pmol added.

both bands when in vitro translation of +42 mRNA was conducted in the presence of [^{14}C]-Leu (Leu codons are present in *tisA* and *tisB*; Figure S1B). The same experiment was carried out with +1, +42, and +106 mRNAs in the presence of either [^{14}C]-Asp or [^{14}C]-Arg, to differentially incorporate amino acids exclusively present either in TisB or TisA. Because inclusion of [^{14}C]-Asp, but not [^{14}C]-Arg, labeled the translation products, only TisB is translated (Figure S1A).

Because the TisA peptide might be unstable in the extract, the entire *tisA* or *tisB* ORF was placed downstream of an artificially introduced heterologous RBS sequence (Figure S1C; *tisA'* and *tisB'*). Figure S1D shows that TisA as well as TisB were detectable. Hence, TisA was stable, and it migrated faster than either of the two TisB-specific products. The translation products of *tisB'*, in contrast, migrated identically to those of active +42 mRNA, implying that only TisB was synthesized. Mutant analysis further supports this conclusion. An early stop codon mutant in *tisB* (Mut-TB; Figure S1D) that does not affect the *tisA* frame failed to produce protein. Translation of N-terminally His-tagged *tisB* (Vogel et al., 2004) resulted in a slower migration of the upper band (data not shown). The weaker TisB-specific band present in Figure 2A and Figures S1A and S1D could be attributed to an alternative start position (AUU; eighth *tisB* codon; Figure 1B). Upon introduction of an AUU>CUU mutation, translation failed to generate the lower band (Figure S1E). Thus, the upper band represents full-length TisB, and the lower one is most likely generated from the alternative start codon.

Translation Initiation Complexes Form Only at the *tisB* RBS

Formation of initiation complexes on mRNAs can be monitored in vitro by reverse transcription; tRNA^{fmet}-dependent 30S ribosome binding to an initiation site gives a "toeprint" signal ~15 nt downstream of the AUG start codon (Hartz et al., 1988). Toeprinting assays were employed to ask (1) whether the different translation activities of the three *tisAB* mRNAs correlated with 30S binding activities and (2) whether translation initiation complexes could form at the putative RBS's of both *tisA* and *tisB*. Strong initiator tRNA-dependent 30S binding to the *tisB* RBS occurred on +42 mRNA, but not on +1 and +106 (Figure 3A), in line with results from the translation assay (Figure 2A). The toeprinting results also confirmed that ribosomes initiated at the *tisB*, but not the *tisA*, RBS. Occasionally, a weak, tRNA-independent, 30S toeprint was observed on +42 mRNA at a position near the *tisA* start codon (see Figure 3A [indicated by bars], middle panel; 10 pmol 30S ± tRNA^{fmet}). The possible significance of this band will be discussed below.

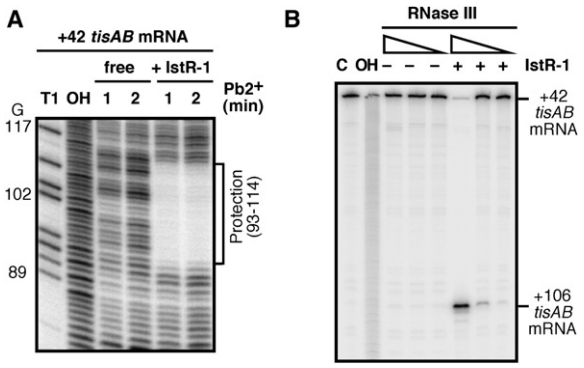

Figure 4. IstR-1 Binding to Its Target Site in *tisAB* mRNA, and RNase III Cleavage of the RNA Duplex

(A) End-labeled +42 *tisAB* mRNA, free or in complex with IstR-1, was subjected to limited lead(II) acetate cleavage for 1 or 2 min. T1, RNase T1 cleavage under denaturing conditions; OH, alkaline ladder. Some nucleotide positions are given for orientation, and the IstR-1-protected region is indicated. Only part of an autoradiogram is shown (see also Figure 6B).

(B) End-labeled +42 *tisAB* mRNA, free or in complex with IstR-1, was treated with three tenfold different concentrations of RNase III. C, control, no treatment, and OH as in (A).

IstR-1 Binding and Cleavage of the Antisense/Target RNA Duplex by RNase III In Vitro

Before carrying out IstR-1-dependent inhibition assays (see below), it was important to assess the in vitro interaction between IstR-1 and its target RNA. Gel-shift assays indicated that IstR-1 binds to +42 mRNA with an association rate constant of $\sim 2 \times 10^5\ M^{-1}\ s^{-1}$ (F.D. and E.G.H.W., unpublished data), similar to values obtained with many antisense/target systems (Wagner et al., 2002). We subjected 5′ end-labeled +42 *tisAB* mRNA, free or in complex with unlabeled IstR-1, to limited lead(II) cleavage analysis. Binding of IstR-1 protected nt 93–114 in *tisAB* mRNA (Figure 4A). An analysis of 5′ end-labeled IstR-1 gave complementary results and showed the 5′ tail and a segment of the first stem loop to take part in base pairing (Figure S2A). Because RNase III is known to cleave the IstrR-1/*tisAB* mRNA complex in vivo (Vogel et al., 2004), we tested whether this ribonuclease would show the same specificity in vitro. When increasing amounts of RNase III were added, no significant cleavages were obtained on free end-labeled +42 mRNA, whereas prior binding of IstR-1 gave a specific cleavage product, +106 mRNA (Figure 4B). The cleavage sites in vivo and in vitro were identical in both participating RNAs (Figure S2B and data not shown).

TisB Translation and Toeprinting Are Specifically Inhibited by IstR-1

Active +42 *tisAB* mRNAs (wild-type and target site mutant Mut-M6) were translated in S30 extracts at increasing concentrations of IstR-1, and inhibition of *tisB* translation was quantitated. Figure 2B shows that IstR-1 at a concentration as low as 60 nM (3-fold excess over target) completely prevented TisB translation from +42 mRNA, in both wild-type/wild-type and Mut-M6/Mut-M6 combinations. When IstR-1 and *tisAB* mRNA combinations contained mismatches (Mut-M6/wild-type; wild-type/Mut-M6; Figure 2C), inhibition was ineffective. Thus, the in vitro results in Figure 2B faithfully reflect the activities of mutant and wild-type RNAs observed in vivo (Vogel et al., 2004).

Toeprinting assays showed the same pattern: $tRNA^{fmet}$-dependent 30S binding to the *tisB* RBS was efficiently inhibited by wild-type, but not Mut-M6, IstR-1 (Figure 3B). When wild-type IstR-1 was bound to the mRNA, this resulted in a strong reverse transcription stop due to the stability of the RNA heteroduplex formed. Note that the position at which IstR-1 is base paired is ~100 nt upstream of the *tisB* RBS.

Secondary Structure Changes at the *tisB* RBS Cannot Account for Differences in +1, +42, and +106 Activity

The in vitro results presented above showed that +42, but not +1 and +106, mRNA was translatable and that IstR-1 inhibited *tisB* translation by binding far upstream of the *tisB* RBS. Because TisA is not translated, regulation of *tisB* via translational coupling is ruled out (see also Discussion). A second model was therefore considered. Secondary or tertiary structure changes—caused either by the different 5′ sequence extensions in the three mRNAs or by binding of IstR-1—might distally affect the accessibility of the *tisB* RBS and, thus, determine whether or not TisB is translated. To test this, we conducted secondary structure predictions, phylogenetic comparisons, and extensive structure probing in vitro. Ribonuclease T1 (specific for unpaired G residues), T2 (unpaired N), V1 (double-stranded, stacked nt), and lead(II) acetate (unstructured nt) were used to induce limited cleavages (<1/RNA molecule) either directly on 5′ end-labeled RNAs or on unlabeled RNAs followed by primer extension analysis for detection of cleavage positions (Experimental Procedures). The secondary structures of the mRNAs are depicted schematically in Figure 5 and are based on the enzymatic and chemical probing results in Figure 6 and Figures S3 and S6. These, and additional experiments (data not shown), indicated that all three mRNAs have virtually identical secondary structures in the 3′ domain downstream of nt 117 (Figure 5). These structures were additionally supported by a phylogenetic comparison (Figure S4). The sequestration of the *tisB* SD in the hairpin between C194 and G210, and the strong stem immediately upstream, is supported by strong cleavages in the apical loop (A201 [second red circle from top]; T2 lanes, Figure 6A) and protections in the stem regions (SD: A206-G210 and upstream stem: T1 and T2; Figure 6A and Figure S3), which are also sites of enhanced cleavage by V1 (V1, Figure 6A). Figure 6B compares all three mRNAs, probed by lead(II), with nucleotide positions side by side (primer extension analysis). We can

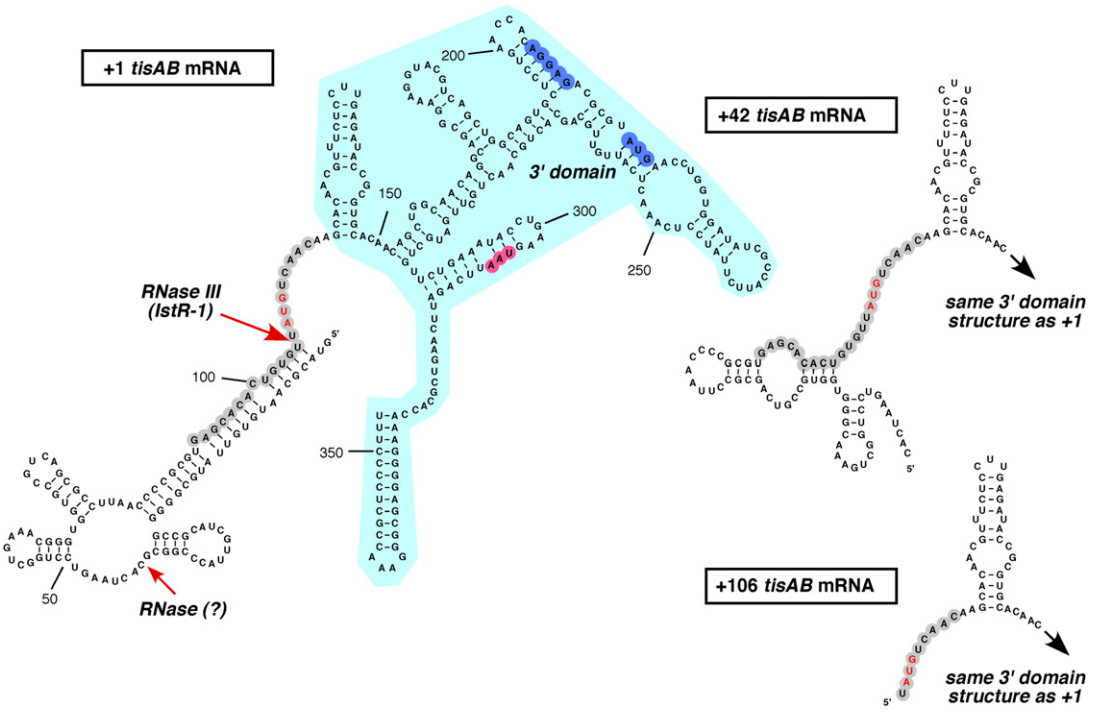

Figure 5. Schematic Representation of *tisAB* mRNA Structures

The secondary structure model of the entire +1 *tisAB* mRNA is shown. The positions of the two experimentally shown cleavages (+42 and +106) are indicated, and some nucleotide positions are given. Nucleotides encircled in gray show the IstR-1 target sequence (*tisA* ORF AUG in red letters). The unchanged 3′ domain (see text) is highlighted in light blue. The *tisB* SD and AUG are indicated as blue circles, and the UAA stop codon in dark red. For +42 and +106 mRNAs, only the different 5′ regions and the first stem loop of the downstream part are shown.

additionally conclude that binding of IstR-1 (Figure 6B, green box) did not cause changes near the *tisB* RBS (Figure 6B, lane + IstR-1). Altogether, this argues against 5′ region-dependent changes in the structures far downstream.

In contrast, the 5′ segments of the RNAs differ (Figure 5). Most structural elements are well supported by mapping. Strong cleavages by either RNase T1, T2, or by lead(II) occur in the loop regions of all stem loops. The region between the 5′ structure of +1 mRNA (nt 1–104) and the first stem of the 3′ domain, which contains part of the IstR-1 target sequence (nt 106–116), is unstructured. The details of the base-pairing scheme between nt 220 and ~260 (Figure 5) are less certain but appear unchanged in the three RNAs (Figure 6B and Figure S6).

From the structure-probing experiments, it follows that the *tisB* SD sequence is sequestered in a stable structure that is present in both the active and the inactive mRNAs. The 5′ domains that contain the entire target sequences (in +1 and +42), or half of it (in +106), differ in sequence and structure. +1 mRNA carries a stable 5′ structure, followed by the unstructured half of the IstR-1 target sequence (Figures 5 and 6). Removal of the first 41 nt rearranges the folding such that the single-stranded (target) stretch becomes extended from 11 to ~15 nt, and moreover, the stem located immediately upstream is unstable. In +106, the single-stranded 11 nt tail is present as in +1, but the entire upstream structure is lacking.

Ribosome Standby on +42 mRNA, and Inhibition of Standby Ribosomes by IstR-1

Based on chemical and enzymatic probing results, differences in the structure encompassing the *tisB* RBS between active and inactive mRNAs, or between IstR-1-bound or free mRNAs, were not supported. In all cases, the *tisB* RBS was sequestered. Nevertheless, ribosomes did access the *tisB* RBS on +42 mRNA (Figure 3). The structural feature that correlates with translatability is the long unstructured/weakly structured 5′ tail, which is only present in the active +42 mRNA but absent in the two inactive mRNAs. Thus, we propose that this accessible region in +42 is a standby site (de Smit and van Duin, 2003; Figure 7). Because ~15 nt are entirely single stranded, and the upstream structure is weak (Figure 5), the 30S subunit could make sequence nonspecific contacts with 35–50 nt (Hüttenhofer and Noller, 1994). The weak signal seen in Figure 3A (bars in middle panel, 10 pmol 30S ± tRNA) might represent a trace of ribosomes on standby.

Following this line of argument, inhibition by IstR-1 is easy to explain (Figure 7): base pairing throughout the target sequence (Figure 4A) blocks the loading site on +42, and inhibition occurs. In line with this, the local

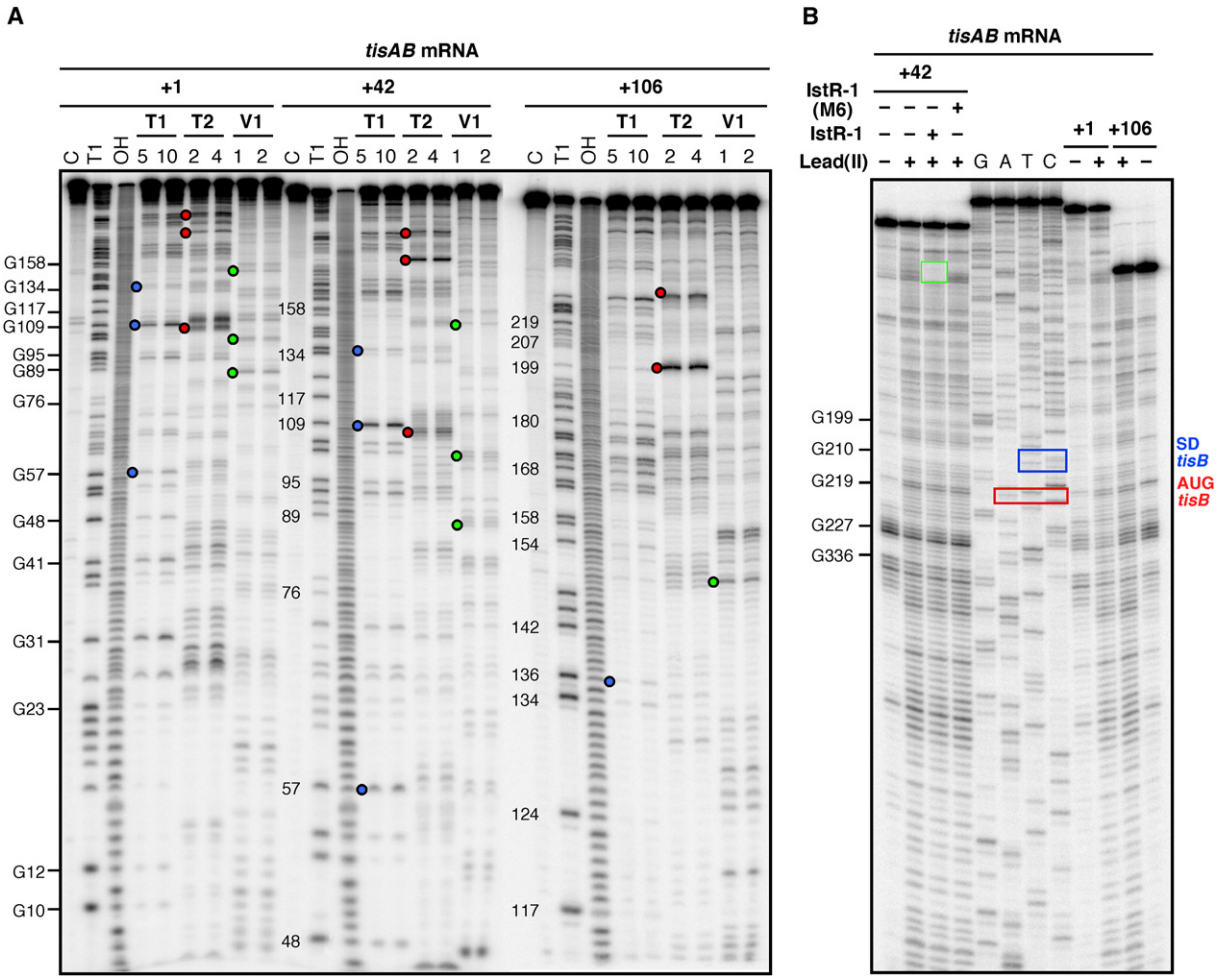

Figure 6. Secondary Structure Mapping of *tisAB* mRNAs

(A) Secondary structure probing of the 5′ end-labeled *tisAB* mRNAs was conducted by limited ribonuclease digestion. For all three RNases, 0.02 U were used per reaction at 37°C in TMN buffer; numbers below enzymes refer to time of cleavage in minutes (see Experimental Procedures). Colored circles are shown for easier comparison of patterns. In each case, the uppermost colored circle in +1, +42, and +104 corresponds to identical nucleotide positions. The positions of several G residues are given. C, control RNA; OH, alkaline ladder; and T1, RNase T1 digestion under denaturing condition.

(B) Lead(II) acetate structure mapping was conducted on unlabeled mRNAs as described in the Experimental Procedures (10 pmol of mRNA/30 μl of TMN buffer). When indicated, 40 pmol of IstR-1 or IstR-1 (Mut-M6) was added to the mRNAs before lead(II) acetate. Reverse transcription was performed on cleaved and control mRNAs with primer PE1 (Table S1). The positions of the *tisB* start codon (red box), SD sequence (blue box), and the IstR-1 protected site (green box) are shown. Several G residues are indicated.

structure around the *tisB* RBS remained unaffected by IstR-1 binding (Figure 6B and Figure S6), yet toeprinting was inhibited (Figure 3B).

A Roadblock between the Standby Site and the *tisB* RBS Inhibits a *tisB* Toeprint

Because direct biochemical evidence for ribosomes on standby was lacking, an indirect experiment was conducted. A deoxyoligoribonucleotide, PE2, was annealed to +42 mRNA between the proposed standby site and the *tisB* RBS structure (Figure 1B), at a distance to interfere neither with standby nor initiation complex formation. Lead(II) cleavages indicated that PE2 binding caused no significant structure change in these regions (Figure S5). Prior binding of PE2 blocks toeprinting at *tisB* as efficiently as does IstR-1 (Figure 3B, cf. lane 3 to lanes 12 and 13). Hence, the oligo appears to act as a roadblock, preventing standby ribosomes from sliding into place upon transient breathing of the *tisB* RBS structure.

Destabilization of the *tisB* RBS Structure Partially Activates +1 and +106 mRNAs

Mutations that disrupt the *tisB* RBS structure should relieve the requirement for standby ribosomes. This is so because destabilization of this structure increases the time window of the unfolded state and consequently

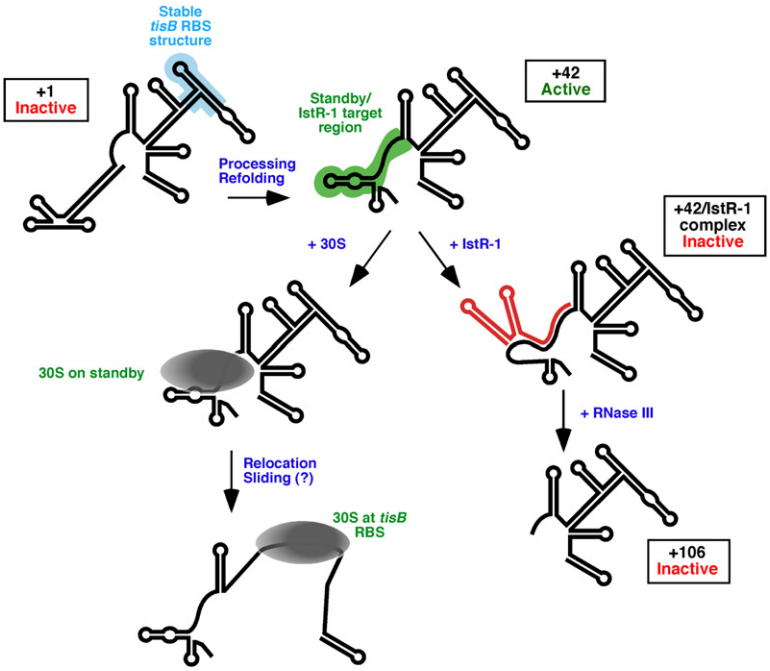

Figure 7. Model of Regulation
This model is based on all the data presented and is described in the text. Simplified structures are based on Figure 5, and translationally active and inactive states of the mRNAs are indicated.

increases the probability for ribosomes to bind directly to the RBS. The RBS mutation (Mut-RBS; Figure 1B) was designed to disrupt base pairing with the *tisB* SD sequence. Enzymatic mapping confirmed that the SD sequence became more accessible in the mutant mRNAs (Figure S6). The translation efficiency of Mut-RBS mRNAs was compared to that of wild-type mRNAs (Figure 2D). Strikingly, destabilization of the local *tisB* SD hairpin in +1 and +106 resulted in significant translation yields (~10% of that obtained with +42). In +42 mRNA, this mutation had very little effect. Thus, when standby binding is permitted, unfolding of the *tisB* RBS structure is not limiting for the initiation rate. Because Mut-RBS +1 and +106 were not restored to 100% translation yield, the local unfolding/folding equilibrium in the mutant RNAs was not increased to a point at which standby binding became inconsequential. Finally, IstR-1 was only partially able to inhibit a toeprint on +42 Mut-RBS mRNA (data not shown).

DISCUSSION

Translation of Structured mRNAs and Standby Ribosomes

Stable RNA structures that sequester SD or entire RBS sequences are a problem for efficient initiation of translation, because ribosomes require this region to be unfolded to gain access and to form the stabilizing anti-SD/SD and initiator tRNA/AUG base-pairing interactions. The ΔG^{o} values of hairpins can be interpreted as K_D values for unfolding/folding reactions. At low K_D values, as in the case of the stable coat gene (MS2 phage) RBS hairpin, calculations indicate that the lifetime of the unfolded hairpin may be as low as 10 μs (at a folding rate of 10^5 s^{-1} [de Smit and van Duin, 2003]). Given the limits for diffusion rates of ribosomes, and the concentration of free ribosomes in cells (~8.5 μM), ribosomes should be virtually unable to translate coat protein. Nevertheless, translation is efficient. This paradox was solved by the ribosome standby model (de Smit and van Duin, 2003). When 30S ribosomes bind unspecifically to single-stranded stretches flanking a structured RBS, the diffusion of ribosomes is no longer limiting and entry to the RBS becomes proportional to the opening/closing equilibrium of the hairpin. Relocation from the standby site to the transiently unfolded RBS may occur by lateral sliding (de Smit and van Duin, 2003; Pavlov et al., 1997). Thus, standby binding is a means to overcome structure at an initiation site, and ribosomal protein S1 (Subramanian, 1983) is probably involved.

The standby model has recently received direct experimental support from fluorescence resonance energy transfer (FRET) studies (Studer and Joseph, 2006). Initiation complex formation on a short, stable RBS-containing hairpin did not occur unless it was preceded by a single-stranded stretch of nucleotides. Two stages were distinguished: an unspecific binding state, which was independent of the SD sequence but inhibited by structure, and stable initiation complex formation once the structure was unfolded. This latter step was affected by the stability of the anti-SD/SD interaction.

The results presented here suggest that, like in the case of the coat hairpin, the *tisB* RBS is structurally sequestered (Figure 6 and Figures S3 and S5). A calculation of the ΔG^{o} of the local structure (Zuker, 2003) gives a value of approximately −16 kcal/ mol at 37°C for the SD hairpin and the bordering upstream stem (see Figure 5), compared to approximately −11 kcal/ mol for the coat RBS

hairpin. Hence, translation of *tisB* should be inhibited by structure. This is indeed the case for +1 and +106 mRNA. However, +42 mRNA is translated (Figure 2A) and gives a toeprint at the *tisB* RBS (Figure 3), even though it displays a 3′ domain structure that is virtually identical to that of the inactive mRNAs. Therefore, the 5′ region of +42 must contain an element responsible for activation. We propose that this region serves as a standby site, because the distinguishing structural difference between the active and the two inactive mRNAs lies in a longer single-stranded stretch of nucleotides bordered by an unstable upstream structure, present only in +42 mRNA. 30S binding and unfolding of the weak structure is consistent with contacts made over 35–50 nt (Hüttenhofer and Noller, 1994). In contrast, the very stable, long 5′ domain of +1 would likely resist unfolding, and the short 5′ tail of +106 would be insufficient to bind ribosomes with reasonable affinity. The standby model is, therefore, entirely in line with the results presented for *tisB* translation (Figure 7) and fully compatible with the patterns of activities seen with the different mRNAs in vivo. For example, a gene encoding only +106 mRNA is nontoxic (Vogel et al., 2004). Induction of a pBAD-promoter-driven +42 mRNA stops cell growth immediately, whereas an induced +1 mRNA gives rise to a 30 min delay before strong toxicity is observed (C.U. and E.G.H.W., unpublished data). This is consistent with +1 initially being inactive in the cell but activated upon processing to +42. Furthermore, evidence for sequestration comes from analysis of Mut-RBS +42 mRNA translation. Upon changes in the nucleotides that base pair with the *tisB* SD sequence (Figures 1B and 7), both +1 and +106 mRNAs became significantly active (Figure 2D). This suggests that direct ribosome binding to the *tisB* RBS is facilitated by structure disruption, and therefore, a partial independence from the standby requirement is obtained. Finally, because toeprinting on +42 mRNA is inhibited when a DNA oligo is base paired between the standby site and the *tisB* RBS structure (Figure 3B), lateral sliding appears to be involved.

Alternative Models

Are there alternative models to account for the differences in translatability between the three mRNAs? We note first that 5′ region-dependent secondary-structure changes that open the *tisB* RBS in +42 mRNA are not supported (Figure 6 and Figures S3 and S6). A second and initially attractive model involves translational coupling between *tisA* and *tisB.* Such a mechanism would readily explain inhibition by IstR-1 (see below), because its binding site overlaps the putative *tisA* start region. Nevertheless, in vivo and in vitro results strongly argue against this. A mutation of the *tisA* start codon did not affect TisB-dependent toxicity in vivo (Vogel et al., 2004), the toeprinting results were obtained in the absence of *tisA* translation (Figure 3), and TisA was not translated in extracts (Figure S1). In addition, a canonical SD sequence with reasonable spacing in front of the *tisA* AUG is absent (Figure 1B), the *tisA* ORF in *Salmonella* spp. is shorter (Vogel et al., 2004), and an ACG sequence replaces the "*tisA*" start codon in *Enterobacter spp.* (Figure S4).

Additional models have been considered but are less plausible. Subtle structural changes involving a pseudoknot formed between upstream sequences available in +42, but not +1 and +106, and sequences at or near the *tisB* RBS could result in translation competence. Long-range interactions, as in the regulation of, e.g., protein L35, have been described (Chiaruttini et al., 1996). We do not favor such a model because good candidates for interactions were not found, nor were corresponding protections detected in our structure mapping.

Inhibition of Standby Binding by IstR-1

Given the standby interpretation for *tisB* translatability, the explanation for inhibition by IstR-1 is straightforward. Base pairing between the two interacting RNAs initiates between the unstructured IstR-1 5′ tail (Figure S1) and the unstructured segment in +42 mRNA and propagates into the weak upstream stem region. For this, the RNA binding protein Hfq is dispensable (C.U., unpublished data). Twenty-one base pairs are formed (Figure 4A), giving a very stable RNA duplex of approximately −36.7 kcal/mol (at 37°C [Hodas and Aalberts, 2004]). Because this renders the standby site double stranded, ribosome loading is efficiently prevented and, consequently, standby-dependent translation of the *tisB* reading frame is inhibited.

Inhibition of translation by IstR-1 is indirect because there is no overlap between the site of antisense RNA binding and the TIR of the target gene. Control systems in which antisense RNA binding occurs far upstream of the TIR of the gene under control are not unusual but have so far involved translational coupling. In plasmid R1 copy number control, CopA (antisense RNA) inhibits *repA* (initiator protein) translation indirectly by blocking translation of the *tap* leader peptide reading frame; translation of *tap* is required to open up the stable *repA* RBS structure, allowing for reinitiation (Blomberg et al., 1992). Translational coupling is also supported in the *hok/sok* TA system ([Gerdes and Wagner, 2007]; see below). A third variant on this theme, involving an activator pseudoknot, was reported for several plasmids (Praszkier and Pittard, 2005). The mechanism is similar to that described for R1. Here, however, translation of a leader peptide opens up the *rep* RBS structure transiently, allowing for formation of a pseudoknot formed between a loop in the antisense target and an anti-SD sequence. This pseudoknot is proposed to maintain a translationally active state, and the antisense RNA competes with pseudoknot formation by binding to the target loop. Thus, to our knowledge, *istR/tisAB* represents the first system in which an antisense RNA regulates a target gene by inhibition of ribosome standby.

Comparisons between the *hok/sok* and *istR/tisAB* TA Systems

The *istR/tisAB* locus encodes a TA system. Many other antisense RNA-controlled TA systems have been

described, with *hok*/*sok* being the founding member (Gerdes and Wagner, 2007). Because this system has been analyzed in mechanistic detail, it is instructive to compare similarities and differences. These systems share no homology and are arranged differently, with Sok being *cis* encoded and IstR-1 *trans* encoded. Both toxins, Hok and TisB, exert toxicity by affecting membranes (Gerdes et al., 1986; C.U., unpublished data). Sok and IstR-1 base pair upstream of the *hok* and *tisB* RBS, respectively, to inhibit toxicity. Both *hok* and *tisAB* mRNAs are extensively base-paired structures that are translationally inert for extended periods of time and require processing to become active; in *hok* mRNA, this involves 3′-terminal trimming, in *tisAB* mRNA endocucleolytic cleavage near the 5′ end. Removal of the tail of *hok* mRNA entails a structural rearrangement that exposes the Sok target stem loop and the TIR of *mok*. Translation of *mok* is translationally coupled to *hok* translation. Similarly, activation of *tisAB* mRNA requires a change in mRNA conformation, but *tisB* is not dependent on translational coupling but rather on ribosome standby. Sok inhibits *mok* translation, whereas IstR-1 inhibits ribosome loading at the standby site. In both cases, antisense-target RNA duplexes are cleaved by RNase III.

Biological Role of *istR*/*tisAB*

The biological role of the plasmid-encoded *hok*/*sok* system is the killing of plasmid-free segregants. In contrast, the chromosomal location of *istR*/*tisAB*, and the induction of *tisB* expression under SOS conditions, suggests that arrested growth, rather than killing, is intended. This would give cells time to recover and carry out DNA repair. Interestingly, there may be redundancy in SOS-associated TA systems. A *relBE*-homologous locus in *E. coli* is preceded by a LexA box, and a second, unrelated TA system, *symR*/*symE*, has recently been discovered (referenced in Gerdes and Wagner [2007]). We suggest that IstR-1 is needed to prevent inadvertent toxicity during normal growth but becomes out-titrated and inactivated when *tisAB* is induced. Thus, upon DNA damage, the system is designed to override the inhibitor.

Conclusions

This new mechanism in which an antisense RNA regulates a target gene by blocking ribosome access to a standby site may be applicable to other control systems as well. For instance, several studies reported inhibition of multiple target genes by induction of single sRNAs (Guillier and Gottesman, 2006; Papenfort et al., 2006; Tjaden et al., 2006). Antisense mechanisms were suspected, yet obvious target sites overlapping TIR sequences were not found. It might therefore be of interest to consider the possibility that target sequences may be located far away from an RBS. If, as proposed by de Smit and van Duin (2003), a standby binding requirement for translation of structured mRNAs is frequent, then many more control systems may employ similar mechanisms as the one described in this work.

EXPERIMENTAL PROCEDURES

Chemicals, Reagents, and Oligodeoxyribonucleotides

Chemicals and reagents were purchased from Sigma-Aldrich or GE-Healthcare unless otherwise specified. Oligodeoxyribonucleotides were from Sigma-Genosys (Table S1).

In Vitro Transcription and 5′ End Labeling

Wild-type and mutant RNAs for structure probing, toeprinting, or in vitro translation experiments were transcribed from PCR fragments generated from *istR*/*tisAB*-carrying plasmid DNA (plasmids in Vogel et al. [2004]). All fragments contain a T7 RNA polymerase promoter sequence. In vitro transcription protocols have been described (Udekwu et al., 2005). Primers used to generate templates for transcription of *tisAB* mRNAs, IstR-1, and Mut-M6 IstR-1 are shown in Table S1. For generation of templates encoding Mut-CUU or Mut-RBS *tisAB* mRNAs, mutagenic oligos (Table S1) were used in a two-step protocol. First, T7+42 (or T7+1, T7+106) and CUUrev (or RBSrev) generated an "upstream" fragment, and 3′tisAB in conjunction with CUUfw (or RBSfw) generated the "downstream" one. Upstream and downstream fragments overlap. After gel purification (Qiagen, QIAEXII), pairs of PCR fragments (200 ng) were annealed at 85°C for 15 min (annealing buffer: 0.1xTE, 0.1 M NaCl [pH 7.5]) and cooled to 30°C. Components were added to obtain a final concentration of 0.2 mM dNTPs, 1xKlenow buffer (Fermentas), and 0.15 U/μl Klenow fragment exo– (Fermentas) to generate transcription templates. After incubation at 37°C for 15 min, samples were treated with phenol-chloroform, ethanol-precipitated, dried, and redissolved in water. Transcripts were dephosphorylated and 5′ end labeled with γ-[^{32}P]-ATP according to the manufacturer's protocol (GE Healthcare).

In Vitro Translation Assays

Translation reactions were performed in *E. coli* S30 extracts (Promega, L1030). Reactions contained the following in a total volume of 25 μl: 0.01–2.5 μM RNA, 0.2 μM [^{35}S]methionine (1000 mCi mmol^{-1}) or 3 μM [^{14} C]leucine (306 mCi mmol^{-1}) or 7 μM [^{14}C]arginine (305 mCi mmol^{-1}) or 10 μM [^{14}C]aspartic acid (205 mCi mmol^{-1}, all from Amersham), 7.5 μl S30 extract, 10 μl S30 premix without amino acids, and 0.1 μM of each amino acid minus either methionine, leucine, arginine, or aspartic acid, respectively. Reaction mixtures were incubated at 37°C for 30 min and analyzed on 15% Tris-Tricine gels (Schagger and von Jagow, 1987). Tricine sample buffer (Biorad, 161-0739) was added, and samples were boiled for 3 min prior to gel loading. Gels were run at 110 V for 3 hr (Biorad, Mini-PROTEAN 3), dried, exposed to PhosphorImager screens for imaging, and band intensities quantified (ImageQuaNT software package, Molecular Dynamics). Rainbow [^{14}C]methylated low-molecular weight proteins (Amersham Biosciences) were used as size marker.

RNA Secondary Structure Probing

Secondary structure probing was conducted on 5′ end-labeled or unlabeled RNAs. Ribonucleases T2 (Invitrogen), T1, and V1 (both from Ambion) were used (Udekwu et al., 2005) at 37°C in TMN buffer (20 mM Tris-acetate [pH 7.5], 5 mM Mg-acetate, and 100 mM Na-acetate). Lead(II) cleavages were done according to Lindell et al. (2002). For labeled RNAs, the reactions were stopped by adding 10 μl of loading buffer II (Ambion). Samples were heated at 95°C for 1 min prior to separation on 6% polyacrylamide/7 M urea gels. Gels were dried and exposed to PhosphorImager screens (see above). Cleavage positions on unlabeled RNA were determined by primer extension analyses using 5′ end-labeled primers PE1 or PE2, according to Lindell et al. (2002). For assignment of nucleotide positions, sequencing reactions were run in parallel with the same primers.

RNase III Cleavage

RNase III (Ambion) cleavage analysis was done as described for secondary structure probing. Incubations were at 37°C for 5 min after

addition of RNase III (0.1, 0.01, or 0.001 U) before stopping the reactions.

Toeprinting Assays

Toeprinting assays were carried out according to Hartz et al. (1988) with minor modifications. Unless specified otherwise, annealing mixtures contained 2 pmol of unlabeled *tisAB* mRNA and 0.5 pmol of 5′ end-labeled PE1 primer in standard buffer (10 mM Tris-acetate [pH 7.6], 0.1 M potassium acetate, and 1 mM DTT). Annealing mixtures were heated for 1 min at 95°C and chilled on ice for 5 min. Magnesium acetate and all NTPs were added to final concentrations of 10 and 1 mM, respectively. For inhibition tests, antisense RNA (IstR-1, IstR-1-M6) or oligo (PE2) was added prior to addition of 30S subunits. After preactivation for 5 min at 37°C, 5 pmol of 30S ribosomal subunits (provided by Ayman Antoun) was added, and incubation continued for 5 min. $tRNA^{fMet}$ (10 pmol) was added, and after 25 min, cDNA was synthesized with Superscript II (200 U, Invitrogen) for 20 min. Reactions were stopped and phenol-chloroform extracted. cDNA was ethanol precipitated and subsequently dissolved in 10 μl of loading buffer II (Ambion). cDNA products were analyzed on 6% polyacrylamide/7 M urea gels. Toeprint signals were identified by comparison to sequences generated with the same 5′ end-labeled primer. Gels were dried and analyzed as above.

Supplemental Data

Supplemental Data include six figures and one table and can be found with this article online at http://www.molecule.org/cgi/content/full/26/3/381/DC1/.

ACKNOWLEDGMENTS

The authors acknowledge support from the Swedish Research Council and the European Commission (EU-STREP FOSRAK and EU-STREP BacRNAs) to E.G.H.W. We thank Ayman Antoun for the generous gift of 30S subunits, Lamine Bouakaz for $tRNA^{fMet}$, and M. Ehrenberg, S. Kuusk, and N. Ausmees for discussions and critically reading the manuscript.

Received: February 21, 2007
Revised: March 25, 2007
Accepted: April 5, 2007
Published: May 10, 2007

REFERENCES

Argaman, L., Hershberg, R., Vogel, J., Bejerano, G., Wagner, E.G.H., Margalit, H., and Altuvia, S. (2001). Novel small RNA-encoding genes in the intergenic regions of Escherichia coli. Curr. Biol. *11*, 941–950.

Blomberg, P., Nordström, K., and Wagner, E.G.H. (1992). Replication control of plasmid R1: RepA synthesis is regulated by CopA RNA through inhibition of leader peptide translation. EMBO J. *11*, 2675–2683.

Chen, S., Lesnik, E.A., Hall, T.A., Sampath, R., Griffey, R.H., Ecker, D.J., and Blyn, L.B. (2002). A bioinformatics based approach to discover small RNA genes in the Escherichia coli genome. Biosystems *65*, 157–177.

Chiaruttini, C., Milet, M., and Springer, M. (1996). A long-range RNA-RNA interaction forms a pseudoknot required for translational control of the IF3-L35-L20 ribosomal protein operon in Escherichia coli. EMBO J. *15*, 4402–4413.

de Smit, M.H., and van Duin, J. (2003). Translational standby sites: how ribosomes may deal with the rapid folding kinetics of mRNA. J. Mol. Biol. *331*, 737–743.

Douchin, V., Bohn, C., and Bouloc, P. (2006). Down-regulation of porins by a small RNA bypasses the essentiality of the regulated intramembrane proteolysis protease RseP in Escherichia coli. J. Biol. Chem. *281*, 12253–12259.

Gerdes, K., and Wagner, E.G.H. (2007). RNA antitoxins. Curr. Opin. Microbiol., in press. Published online March 19, 2007. 10.1016/ j. mib.2007.03.003.

Gerdes, K., Bech, F.W., Jörgensen, S.T., Löbner-Olesen, A., Rasmussen, P.B., Atlung, T., Boe, L., Karlstrom, O., Molin, S., and von Meyenburg, K. (1986). Mechanism of postsegregational killing by the hok gene product of the parB system of plasmid R1 and its homology with the relF gene product of the E. coli relB operon. EMBO J. *5*, 2023–2029.

Gerdes, K., Gultyaev, A.P., Franch, T., Pedersen, K., and Mikkelsen, N.D. (1997). Antisense RNA-regulated programmed cell death. Annu. Rev. Genet. *31*, 1–31.

Gottesman, S. (2004). The small RNA regulators of Escherichia coli: roles and mechanisms. Annu. Rev. Microbiol. *58*, 303–328.

Guillier, M., and Gottesman, S. (2006). Remodelling of the Escherichia coli outer membrane by two small regulatory RNAs. Mol. Microbiol. *59*, 231–247.

Guillier, M., Gottesman, S., and Storz, G. (2006). Modulating the outer membrane with small RNAs. Genes Dev. *20*, 2338–2348.

Hartz, D., McPheeters, D.S., Traut, R., and Gold, L. (1988). Extension inhibition analysis of translation initiation complexes. Methods Enzymol. *164*, 419–425.

Hauryliuk, V., and Ehrenberg, M. (2006). Two-step selection of mRNAs in initiation of protein synthesis. Mol. Cell *22*, 155–156.

Hodas, N.O., and Aalberts, D.P. (2004). Efficient computation of optimal oligo-RNA binding. Nucleic Acids Res. *32*, 6636–6642.

Huntzinger, E., Boisset, S., Saveanu, C., Benito, Y., Geissmann, T., Namane, A., Lina, G., Etienne, J., Ehresmann, B., Ehresmann, C., et al. (2005). Staphylococcus aureus RNAIII and the endoribonuclease III coordinately regulate spa gene expression. EMBO J. *24*, 824–835.

Hüttenhofer, A., and Noller, H.F. (1994). Footprinting mRNA-ribosome complexes with chemical probes. EMBO J. *13*, 3892–3901.

Lindell, M., Romby, P., and Wagner, E.G.H. (2002). Lead(II) as a probe for investigating RNA structure in vivo. RNA *8*, 534–541.

Massé, E., and Gottesman, S. (2002). A small RNA regulates the expression of genes involved in iron metabolism in Escherichia coli. Proc. Natl. Acad. Sci. USA *99*, 4620–4625.

Morita, T., Mochizuki, Y., and Aiba, H. (2006). Translational repression is sufficient for gene silencing by bacterial small noncoding RNAs in the absence of mRNA destruction. Proc. Natl. Acad. Sci. USA *103*, 4858–4863.

Papenfort, K., Pfeiffer, V., Mika, F., Lucchini, S., Hinton, J.C., and Vogel, J. (2006). sigma(E)-dependent small RNAs of Salmonella respond to membrane stress by accelerating global omp mRNA decay. Mol. Microbiol. *62*, 1674–1688.

Pavlov, M.Y., Freistroffer, D.V., MacDougall, J., Buckingham, R.H., and Ehrenberg, M. (1997). Fast recycling of Escherichia coli ribosomes requires both ribosome recycling factor (RRF) and release factor RF3. EMBO J. *16*, 4134–4141.

Praszkier, J., and Pittard, A.J. (2005). Control of replication in I-complex plasmids. Plasmid *53*, 97–112.

Rasmussen, A.A., Eriksen, M., Gilany, K., Udesen, C., Franch, T., Petersen, C., and Valentin-Hansen, P. (2005). Regulation of ompA mRNA stability: the role of a small regulatory RNA in growth phase-dependent control. Mol. Microbiol. *58*, 1421–1429.

Repoila, F., Majdalani, N., and Gottesman, S. (2003). Small non-coding RNAs, co-ordinators of adaptation processes in Escherichia coli: the RpoS paradigm. Mol. Microbiol. *48*, 855–861.

Rivas, E., Klein, R.J., Jones, T.A., and Eddy, S.R. (2001). Computational identification of noncoding RNAs in E. coli by comparative genomics. Curr. Biol. *11*, 1369–1373.

Romby, P., Vandenesch, F., and Wagner, E.G.H. (2006). The role of RNAs in the regulation of virulence-gene expression. Curr. Opin. Microbiol. *9*, 229–236.

Schagger, H., and von Jagow, G. (1987). Tricine-sodium dodecyl sulfate-polyacrylamide gel electrophoresis for the separation of proteins in the range from 1 to 100 kDa. Anal. Biochem. *166*, 368–379.

Storz, G., Altuvia, S., and Wassarman, K.M. (2005). An abundance of RNA regulators. Annu. Rev. Biochem. *74*, 199–217.

Studer, S.M., and Joseph, S. (2006). Unfolding of mRNA secondary structure by the bacterial translation initiation complex. Mol. Cell *22*, 105–115.

Subramanian, A.R. (1983). Structure and functions of ribosomal protein S1. Prog. Nucleic Acid Res. Mol. Biol. *28*, 101–142.

Tjaden, B., Goodwin, S.S., Opdyke, J.A., Guillier, M., Fu, D.X., Gottesman, S., and Storz, G. (2006). Target prediction for small, noncoding RNAs in bacteria. Nucleic Acids Res. *34*, 2791–2802.

Udekwu, K.I., Darfeuille, F., Vogel, J., Reimegård, J., Holmqvist, E., and Wagner, E.G.H. (2005). Hfq-dependent regulation of OmpA synthesis is mediated by an antisense RNA. Genes Dev. *19*, 2355–2366.

Valentin-Hansen, P., Eriksen, M., and Udesen, C. (2004). The bacterial Sm-like protein Hfq: a key player in RNA transactions. Mol. Microbiol. *51*, 1525–1533.

Vogel, J., and Papenfort, K. (2006). Small non-coding RNAs and the bacterial outer membrane. Curr. Opin. Microbiol. *9*, 605–611.

Vogel, J., Bartels, V., Tang, T.H., Churakov, G., Slagter-Jäger, J.G., Hüttenhofer, A., and Wagner, E.G.H. (2003). RNomics in Escherichia coli detects new sRNA species and indicates parallel transcriptional output in bacteria. Nucleic Acids Res. *31*, 6435–6443.

Vogel, J., Argaman, L., Wagner, E.G.H., and Altuvia, S. (2004). The small RNA IstR inhibits synthesis of an SOS-induced toxic peptide. Curr. Biol. *14*, 2271–2276.

Wagner, E.G.H., and Darfeuille, F. (2006). Small regulatory RNAs in bacteria. In Small RNAs: Analysis and Regulatory Functions, W. Nellen, and C. Hammann, eds. (Berlin: Springer Verlag), pp. 1–30.

Wagner, E.G.H., Altuvia, S., and Romby, P. (2002). Antisense RNAs in bacteria and their genetic elements. Adv. Genet. *46*, 361–398.

Wassarman, K.M., Repoila, F., Rosenow, C., Storz, G., and Gottesman, S. (2001). Identification of novel small RNAs using comparative genomics and microarrays. Genes Dev. *15*, 1637–1651.

Zuker, M. (2003). Mfold web server for nucleic acid folding and hybridization prediction. Nucleic Acids Res. *31*, 3406–3415.